

First time-dependent study of H_2 and H_3^+ *ortho*–*para* chemistry in the diffuse interstellar medium: observations meet theoretical predictions¹

T. Albertsson¹, N. Indriolo², H. Kreckel³, D. Semenov¹, K. N. Crabtree⁴ and Th. Henning¹

(1) *Max-Planck-Institut für Astronomie, Königstuhl 17, 69117 Heidelberg, Germany*

(2) *Department of Physics and Astronomy, Johns Hopkins University, Baltimore, MD 21218, USA*

(3) *Max-Planck-Institut für Kernphysik, 69117 Heidelberg, Germany*

(4) *Harvard–Smithsonian Center for Astrophysics, 60 Garden St., Cambridge, MA 02138, USA*

ABSTRACT

The chemistry in the diffuse interstellar medium initiates the gradual increase of molecular complexity during the life cycle of matter. A key molecule that enables build-up of new molecular bonds and new molecules via proton-donation is H_3^+ . Its evolution is tightly related to molecular hydrogen and thought to be well understood. However, recent observations of *ortho* and *para* lines of H_2 and H_3^+ in the diffuse ISM showed a puzzling discrepancy in nuclear spin excitation temperatures and populations between these two key species. H_3^+ , unlike H_2 , seems to be out of thermal equilibrium, contrary to the predictions of modern astrochemical models. We conduct the first time-dependent modeling of the *para*-fractions of H_2 and H_3^+ in the diffuse ISM and compare our results to a set of line-of-sight observations, including new measurements presented in this study. We isolate a set of key reactions for H_3^+ and find that the destruction of the lowest rotational states of H_3^+ by dissociative recombination largely control its *ortho/para* ratio. A plausible agreement with observations cannot be achieved unless a ratio larger than 1:5 for the destruction of (1, 1)– and (1, 0)–states of H_3^+ is assumed. Additionally, an increased CR ionization rate to 10^{-15} s^{-1} further improves the fit whereas variations of other individual physical parameters, such as density and chemical age, have only a minor effect on the predicted *ortho/para* ratios. Thus our study calls for new laboratory measurements of the dissociative recombination rate and branching ratio of the key ion H_3^+ under interstellar conditions.

Subject headings: astrochemistry - molecular processes - spin states - methods: numerical, molecules, abundances - diffuse molecular cloud

¹Partly based on observations collected at the European Organization for Astronomical Research in the Southern Hemisphere, Chile, as part of program 088.C-0351

1. Introduction

H_3^+ plays a pivotal role in the gas-phase chemistry of the interstellar medium due to its very low proton affinity, allowing it to transfer a proton to many neutral atoms and molecules (exception being N and O_2). The chemistry of H_3^+ is straightforward. The formation process via the ion-molecule reaction $\text{H}_2^+ + \text{H}_2 \rightarrow \text{H}_3^+ + \text{H}$ is well-established (e.g. Liszt 2006). The destruction of H_3^+ can occur via ion-molecule reactions or dissociative recombination (DR) with free electrons. Under typical conditions of different ISM environments H_3^+ was long believed to exist below observable limits. Still, H_3^+ was observed in the interstellar medium by Geballe & Oka (1996) for the first time, followed by other detections (e.g. McCall et al. 1998; Geballe et al. 1999; McCall et al. 2002; Goto et al. 2008; Indriolo et al. 2007; Indriolo & McCall 2012). These observations have also revealed several unexpected results, which are summarized below.

In the simple gas-phase chemistry of H_3^+ only three parameters can strongly affect its steady-state abundance: the dissociative recombination rate coefficients, the electron abundance, and the cosmic-ray (CR) ionization rate (McCall et al. 2003). The former two parameters are thought to be well constrained in diffuse interstellar clouds (Cardelli et al. 1996; McCall et al. 2003), which leaves the CR ionization rate as the only controlling parameter. McCall et al. (2003), Indriolo et al. (2007) and Indriolo & McCall (2012) observed absorption lines of H_3^+ toward several diffuse cloud sight lines, and inferred CR ionization ratios on the order of $\sim 10^{-16} \text{ s}^{-1}$, about an order of magnitude higher than the value inferred for dark prestellar cores ($\sim 10^{-17} \text{ s}^{-1}$, see e.g. Webber 1998; van der Tak & van Dishoeck 2000; Caselli 2003; van der Tak 2006). If one relaxes the steady-state approximation, the density starts to play an important role in the H_3^+ evolution (see e.g. Cecchi-Pestellini et al. 2009; Falgarone et al. 2013).

Furthermore, observations of the average excitation temperature derived from the two lowest rotational states of H_3^+ , $T(\text{H}_3^+) \approx 30 \text{ K}$ (Indriolo et al. 2007; Indriolo & McCall 2012). It differs significantly from that of the two lowest rotational states of H_2 , $T_{01} \approx 70 \text{ K}$ (Rachford et al. 2002, 2009). Because the conversion between the two lowest nuclear spin states of H_2 in collisions with free protons is very efficient, the H_2 *ortho*–*para* ratio is expected to be thermalized with the gas kinetic temperature. Hence, the excitation temperature derived from the relative intensities of H_2 *ortho* and *para* levels are also expected to be an accurate measure of the gas kinetic temperature in the diffuse ISM ($\approx 70 \text{ K}$). Assuming that collisional thermalization between H_3^+ and H_2 is also efficient, in previous studies by McCall et al. (2003) and Gibb et al. (2010) the nuclear spin states of H_3^+ were assumed to be in thermal equilibrium with the kinetic cloud temperature. However, in later studies the excitation temperatures of H_2 and H_3^+ directly derived from observations did not agree with each other, indicating that a large population of H_3^+ is not thermalized with the diffuse ISM gas.

Crabtree et al. (2011) have investigated this discrepancy by comparing observations of the nuclear spin temperature of H_3^+ (subsequently refined by Indriolo & McCall 2012) to that of H_2 for a sample of diffuse interstellar clouds. Their results confirmed that the excitation temperature of H_3^+ and H_2 do not agree. Crabtree et al. (2011) concluded that the H_3^+ *ortho/para* ratio is likely governed by a competition between the collisionally-driven thermalization of H_3^+ and the DR reactions with electrons. The thermalization reaction *ortho/para*– $\text{H}_3^+ + \text{H}_2 \rightarrow$ *ortho/para* $\text{H}_3^+ + \text{H}_2$ has recently been studied experimentally by Grussie et al.

(2012). It was found that the reaction has indeed the expected thermal outcome.

From a theoretical point of view, there are more unknown factors related to the chemistry of H_3^+ . Theoretical calculations have shown that the photodissociation of H_3^+ is not efficient in the diffuse interstellar medium (see e.g. van Dishoeck 1987). In the absence of other abundant molecules like CO and H_2O , this leaves DR as the only major destruction pathway for H_3^+ . Recent theoretical calculations by dos Santos et al. (2007) predict the DR rate coefficient for *para*- H_3^+ at low temperature to be an order of magnitude higher than that for *ortho*- H_3^+ . This claim has later been backed up by the plasma experiments of Varju et al. (2011). Meanwhile, other laboratory groups have observed a different dependence, with similar dissociation rates between the two nuclear spin states of H_3^+ (see e.g. Kreckel et al. 2005; Tom et al. 2009; Kreckel et al. 2010).

In this paper we conduct the first time-dependent study of the *ortho*-*para* chemistry of H_3^+ in the diffuse interstellar medium. We isolate a set of key processes for the evolution of the *ortho*- and *para*-states of H_3^+ , and we present new observational measurements to better test our model predictions. The paper is structured as follows. In Section 2 we discuss the new observations. In Section 3 we describe the chemical and physical models utilized in the analysis of the observations. Our results and the underlying chemistry is presented and discussed in Section 4, followed by conclusions given in Section 5.

2. Observations

Following the initial comparison of the H_3^+ and H_2 *ortho/para* ratios presented by Crabtree et al. (2011) we proposed new observations of H_3^+ in eight diffuse cloud sight lines with measured H_2 column densities. The intent of these new observations was to significantly expand the sample size from the five sight lines considered by Crabtree et al. (2011). Targeted sight lines were selected based on large observed H_2 column densities ($N(\text{H}_2) > 10^{20} \text{ cm}^{-2}$ Rachford et al. 2002, 2009; Savage et al. 1977), and bright infrared background sources ($L > 7.5 \text{ mag}$) to maximize the likelihood of H_3^+ detections with relatively short ($\lesssim 2 \text{ hr}$) exposure times. Despite these considerations, H_3^+ absorption lines were detected in only three of the eight targeted sight lines. As the new H_3^+ detections are relevant to the current study, they are presented herein, whereas the non-detections will be presented in a future publication.

The sight lines toward HD 27778, HD 43384, and HD 41117 were observed on 2011 Nov 6, 2011 Dec 1, and 2012 Apr 1, respectively, using the Cryogenic High-resolution Infrared Echelle Spectrograph (CRIRES; Kaeufl et al. 2004) on UT1 at the Very Large Telescope. Observations were performed in service mode, and CRIRES was used with its $0''.2$ slit to provide a resolving power (resolution) of about 100,000 (3 km s^{-1}), and a reference wavelength of 3715.0 nm to position the H_3^+ $R(1, 1)^l$ ($\lambda = 3.715479 \mu\text{m}$) transition on detector 3, and the $R(1, 1)^u$ ($\lambda = 3.668083 \mu\text{m}$) and $R(1, 0)$ ($\lambda = 3.668516 \mu\text{m}$) transitions on detector 1. The adaptive optics system was utilized in all cases to maximize starlight passing through the narrow slit. Spectra were obtained in an ABBA pattern with $10''$ between the two nod positions and $\pm 3''$ jitter width. Total integration times for the three targets were as follows: HD 27778: 34 min; HD 43384: 12 min; HD 41117: 12 min.

Raw data images were processed using the CRIRES pipeline version 2.2.1. Standard calibration tech-

niques, including subtraction of dark frames, division by flat fields, interpolation over bad pixels, and correction for detector non-linearity effects, were utilized. Consecutive A and B nod position images were subtracted from each other to remove sky emission features. One-dimensional spectra were extracted from these images using the *apall* routine in IRAF², and any remaining bad pixels were interpolated over. Spectra were then imported to Igor Pro³, and all spectra from each nod position were added together. Wavelength calibration of the summed A and summed B spectra was performed using atmospheric absorption lines (accurate to $\pm 1 \text{ km s}^{-1}$), after which the spectra from the A and B nod positions were averaged onto a common wavelength scale.⁴ In order to remove atmospheric absorption features, science target spectra were divided by spectra of telluric standard stars. Resulting spectra are shown in Figure 1.

Absorption features due to H_3^+ were fit with Gaussian functions for the purpose of determining equivalent widths, velocity FWHM, and interstellar gas velocities. Equivalent widths were used to compute column densities in the lower state, and the *para*- H_3^+ column density was then determined by taking a variance-weighted average of the values found from the $R(1, 1)^u$ and $R(1, 1)^l$ transitions. As we in this paper will discuss our results in terms of the *para*-to-total ratio (*para* fraction), we here define these parameters for H_2 and H_3^+ as:

$$p_2 = [\textit{para} - \text{H}_2]/[\text{H}_2]$$

$$p_3 = [\textit{para} - \text{H}_3^+]/[\text{H}_3^+]$$

All of the absorption line parameters and derived column densities are presented in Table 1, along with the inferred p_3 and excitation temperatures, $T(\text{H}_3^+)$. Also shown are H_2 column densities, H_2 *para* fractions (p_2), and T_{01} presented in Rachford et al. (2002, 2009).

The three new detections of H_3^+ presented in this paper increase the total number of diffuse cloud sight lines with measurements of column densities of the *ortho* and *para* forms of both H_3^+ and H_2 from six to nine. Two of these sight lines—HD 27778 and HD 41117⁵—were observed previously but H_3^+ was not detected (McCall et al. 2002; Indriolo & McCall 2012). Column densities in the (1,0) and (1,1) levels reported in this paper are consistent with the previously reported upper limits. The newly reported values of p_3 and p_2 follow the same trend shown by the six older data points in Crabtree et al. (2011) and Crabtree & McCall (2012). This continues to demonstrate that in diffuse clouds the excitation temperatures of H_2 and H_3^+ do not agree with each other, even when both species are observed in the same line of sight. This developing trend, and the lack of an adequate explanation from simple chemical models, is part of the reason for the present study.

²<http://iraf.noao.edu/>

³<http://www.wavemetrics.com/>

⁴Combination of A and B spectra is done after wavelength calibration due to a slight (about one-half pixel) shift in wavelength along the dispersion direction between the two nod positions.

⁵Note that these sight lines are frequently referred to by the alternate identifiers 62 Tau and χ^2 Ori, respectively.

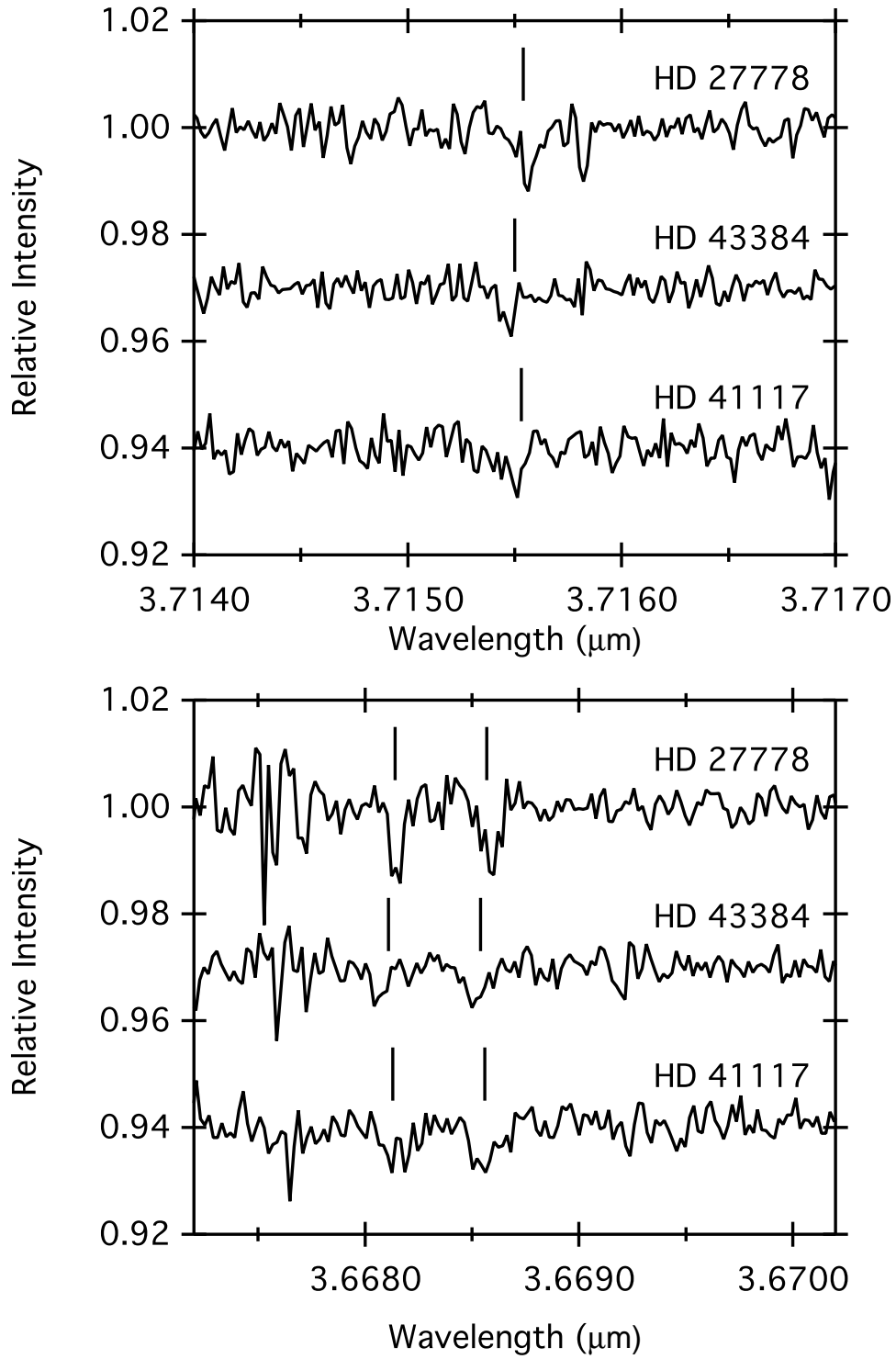


Fig. 1.— Spectra of HD 27778, HD 43384, and HD 41117 showing absorption due to the $R(1,1)''$ and $R(1,0)$ (bottom) and $R(1,1)'$ (top) transitions of H_3^+ . Vertical lines above spectra mark the expected positions of absorption features given previously determined interstellar gas velocities.

Table 1. Absorption line parameters and derived values

		HD 27778 ^a	HD 41117 ^b	HD 43384 ^b
$v_{\text{LSR}} R(1, 1)^u$	(km s ⁻¹)	5.2	5.7	-1.5
$v_{\text{LSR}} R(1, 0)$	(km s ⁻¹)	5.9	2.5	-0.1
$v_{\text{LSR}} R(1, 1)^l$	(km s ⁻¹)	6.9	2.2	-0.8
<i>FWHM</i> $R(1, 1)^u$	(km s ⁻¹)	4.7	8.4	5.6
<i>FWHM</i> $R(1, 0)$	(km s ⁻¹)	6.5	7.4	8.5
<i>FWHM</i> $R(1, 1)^l$	(km s ⁻¹)	7.3	4.9	5.4
$W_\lambda R(1, 1)^u$	(10 ⁻⁶ μm)	0.93±0.14	1.11±0.23	0.49±0.11
$W_\lambda R(1, 0)$	(10 ⁻⁶ μm)	1.00±0.17	0.82±0.20	0.73±0.15
$W_\lambda R(1, 1)^l$	(10 ⁻⁶ μm)	0.91±0.21	0.56±0.15	0.55±0.13
$N(J, K) R(1, 1)^u$	(10 ¹³ cm ⁻²)	3.87±0.58	4.60±0.97	2.03±0.47
$N(J, K) R(1, 0)$	(10 ¹³ cm ⁻²)	2.53±0.42	2.07±0.52	1.85±0.37
$N(J, K) R(1, 1)^l$	(10 ¹³ cm ⁻²)	4.18±0.94	2.55±0.68	2.54±0.62
$N(1, 1) - \text{H}_3^+$	(10 ¹³ cm ⁻²)	3.96±0.22	3.22±1.45	2.22±0.36
$N(1, 0) - \text{H}_3^+$	(10 ¹³ cm ⁻²)	2.53±0.42	2.07±0.52	1.85±0.37
p_3		0.61±0.04	0.61±0.12	0.55±0.06
$T(\text{H}_3^+)$	(K)	29±4	29±13	38±11
$\log[N(0)] - \text{H}_2$		20.64±0.05	20.51±0.10	20.59±0.10
$\log[N(1)] - \text{H}_2$		20.27±0.10	20.22±0.10	20.54±0.18
p_2		0.70±0.05	0.66±0.07	0.53±0.12
T_{01}	(K)	56±5	60±7	74±15

3. Model

3.1. Physical model

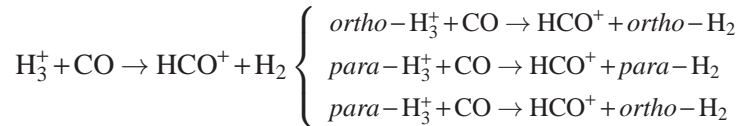
We have utilized the gas-grain chemical model “ALCHEMIC” developed by Semenov et al. (2010), where a detailed description of the code and its performance is presented. Below we give a brief explanation of the code. In these low-density environments, surface interaction is not expected to play an important role in the chemistry. Never the less this is included in our model and explained in detail in Semenov et al. (2010).

To calculate UV ionization and dissociation rates, several tens of photoreaction rates are updated using the calculations of van Dishoeck et al. (2006). A UV photodesorption yield for surface species of 10^{-3} is assumed (see e.g. Öberg et al. 2009b,a). The self-shielding of H_2 from photodissociation is calculated by Eq. (37) from Draine & Bertoldi (1996), assuming a total extinction of 0.5 mag with $N(H) \approx 1.6 \times 10^{21} \text{ cm}^{-2}$, resulting in a $N(H_2) \approx 4 \times 10^{20} \text{ cm}^{-2}$. The shielding of CO by dust grains, H_2 , and its self-shielding is calculated using the precomputed table of Lee et al. (1996, see Table 11).

In this work we are primarily concerned with reproducing observed *ortho*- and *para*-abundances of H_3^+ and H_2 . We conduct a parametric study using our time-dependent chemical model. For this goal, gas density, DR and CR ionization rates, as well as initial *ortho/para* ratio of H_2 and chemical age, are varied within the ranges typical of the diffuse ISM, and the modeled p_2 and p_3 values are compared with the observed values. There are still large uncertainties as to the initial abundances in diffuse clouds, concerning especially the depletion factor of metals and the degree of ionization (see e.g. Le Bourlot et al. 1995; Snow & McCall 2006; Jenkins 2009). To study the impact of different initial abundances we implement both the “low metal” and “high metal” abundances from Graedel et al. (1982) and Lee et al. (1998). Furthermore, we consider the neutral and fully ionized cases of initial abundances. Diffuse molecular clouds have typical densities of 10 - 100 cm^{-3} with typical extinction of $A_V = 0.5 \text{ mag}$ (Snow & McCall 2006). The CR ionization rate in the diffuse ISM is a matter of debate (see e.g. Indriolo et al. 2007, 2009; Rimmer et al. 2012; Indriolo & McCall 2012). It is clear that the CR ionization rate plays a crucial role in the chemical evolution owing to its importance in the formation of H_3^+ through the ionization of H_2 and it also has a significant effect on the *para*-fractions of H_2 and H_3^+ . Therefore we consider a wide range of CR ionization rates between $10^{-17} - 10^{-15} \text{ s}^{-1}$. The lifetime of giant molecular clouds is typically in the range of several 10^7 years (McKee & Ostriker 2007), giving us an upper limit for the time scales of diffuse cloud evolution. Our cloud models are calculated within a time span of 10^6 years, but we also investigate the time effects on results for longer time spans of 10^7 years. As a “Standard” model (“S”) we consider a hydrogen gas density $n_H = 10 \text{ cm}^{-3}$, $\zeta_{CR} = 10^{-16} \text{ s}^{-1}$, $A_V = 0.5 \text{ mag}$, and temperatures 10–100 K, adopting the H_3^+ DR rates of McCall et al. (2004). The initial *ortho/para* ratio of H_2 is still unknown for the ISM, therefore we investigate two values: 1:10, characteristic of low temperatures, and 3:1, the value characteristic for warm temperatures $\gtrsim 100 \text{ K}$ (see e.g. Sternberg & Neufeld 1999; Pagani et al. 2011).

3.2. Chemical network

We used a smaller version of the chemical network developed by Albertsson et al. (2013), which is based on the `osu.2007` ratfile with recent updates to reaction rates, which we have modified such as only H-bearing reactions with < 4 H atoms, < 4 C atoms and molecules made of < 8 atoms are cloned. In this study we extended it to include the *ortho-para* states of H_2 , H_2^+ and H_3^+ , and related nuclear spin-state exchange processes. Reaction rates for a small number of reactions have already been measured or theoretically predicted. For this, we have added rates from several sources (Gerlich 1990; Walmsley et al. 2004; Flower et al. 2004; Pagani et al. 2009; Honvault et al. 2011), including reaction rates for the $\text{H}_3^+ + \text{H}_2$ system by Hugo et al. (2009). For any remaining reactions involving H_2 , H_2^+ , or H_3^+ with unknown rates, we extracted reactions containing these species and employed a separation scheme, similar to that from Sipilä et al. (2013), in order to generate *ortho-* and *para-*variations of the reactions. We illustrate the process of our separation scheme with the following example:



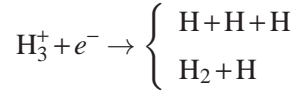
where the left side is the original reaction, and the right shows the pathways resulting from the separation scheme. The reaction rate R is the same as the original rate R_{org} for the first pathway, while the reaction for *para*- H_3^+ has two possible sets of products, and the reaction rate is divided between the two pathways, $R_{\text{org}}/2$. This branching ratio is due to spin statistics (see e.g. Crabtree & McCall 2013; Okumura et al. 2013). Contrary to Sipilä et al. (2013), we allow reactions without H_3^+ or H_2^+ as reactants to form not only *para*- H_2 , but also *ortho*- H_2 with an energy barrier of $\gamma = 170$ K. The final network consists of 1 300 species connected by 40 000 reactions. This networks includes gas-grain interactions and surface reactions. We assume that H_2 is formed with a 3:1 *ortho:para* ratio, aligned with what is generally assumed in models and also supported by the first confirmation from laboratory experiments (Watanabe et al. 2010). However, the *ortho-para* interconversion on dust surfaces are still highly uncertain (Chehrouri et al. 2011). In Table 2 we summarize the different models used to study the effects of physical and chemical parameters.

Table 2. Summary of studied models.

Model	n_{H} [cm^{-3}]	CR rate [s^{-1}]	Time [years]	DR rates [reference]	Initial H_2 o:p
S	10	10^{-16}	10^6	McCall et al. (2004)	1:10
N100	100	10^{-16}	10^6	McCall et al. (2004)	1:10
N1000	1000	10^{-16}	10^6	McCall et al. (2004)	1:10
C15	10	10^{-15}	10^6	McCall et al. (2004)	1:10
C17	10	10^{-17}	10^6	McCall et al. (2004)	1:10
T	10	10^{-16}	10^7	McCall et al. (2004)	1:10
D	10	10^{-16}	10^6	dos Santos et al. (2007)	1:10
O	10	10^{-16}	10^6	McCall et al. (2004)	3:1
2X	10	10^{-16}	10^6	$2 \times$ McCall et al. (2004)	1:10

3.2.1. H_3^+ dissociative recombination

One of the crucial reactions for the hydrogen chemistry in the diffuse interstellar gas is the DR of H_3^+ with free electrons:



The DR process is one of the dominant destruction processes for H_3^+ in the environments considered here, it influences the ionization balance by removing the reactive H_3^+ ion and yielding neutral fragments. Owing to its astrophysical relevance, the DR of H_3^+ is a much-studied process, both experimentally and theoretically. The outcome of H_3^+ DR studies has varied over the years, and to date there are more than 30 published experimental rate coefficients for this reaction. Historically, there were orders of magnitude discrepancies between different experimental approaches at times, with flowing and stationary afterglow experiments resulting in substantially lower rates than storage ring experiments, which have become the prevalent method for DR studies since the early nineties. However, the afterglow experiments have been re-evaluated recently (Glosík et al. 2009), and the inclusion of ternary collisions in the analysis has led to a good overall agreement between different methods concerning the absolute scale of the low-energy rate coefficient for H_3^+ . A review on the early measurements and disagreements can be found in Larsson (2000); here we will focus on the current state-of-the-art and the best rate coefficient to use for our purpose.

The commonly accepted experimental value for the absolute DR rate is given as a thermal rate coefficient in McCall et al. (2004), as a function of temperature:

$$r_{\text{DR,McCall}} = -1.3 \times 10^{-8} + 1.27 \times 10^{-6} T^{-0.48} \quad (1)$$

The underlying measurements were carried out using a supersonic expansion ion source at the CRYRING storage ring and confirmed over a wide range of relative energies by subsequent measurements at the Test Storage Ring (TSR) in Heidelberg (Kreckel et al. 2005, 2010). However, the latest of these studies (Kreckel et al. 2010; Petrigani et al. 2011) revealed that the expansion ion source delivered much hotter ions than previously assumed, and the best characterized measurements were carried out at ~ 370 K (Petrignani et al. 2011). The implications for the rate coefficient at $T < 100$ K are uncertain.

Theoretically, the DR of H_3^+ has proven difficult to describe. The classical picture of direct DR that proceeds through a curve-crossing of a dissociative state does not apply for H_3^+ , and thus initial studies predicted a very low rate coefficient. This picture has changed when more modern studies in full-dimensionality became available and identified the Jahn-Teller effect as the driving force behind H_3^+ DR (Kokoouline et al. 2001; Kokoouline & Greene 2003a,b). With these major advances, the more recent calculations of dos Santos et al. (2007) agree quite well with the storage ring measurements for the absolute recombination rate, while discrepancies remain for the detailed energy-dependence (Petrignani et al. 2011). We adopt rate coefficients converted to the Kooji formulation, by adjusting the coefficients for best agreement in our temperature range of 10–100 K:

$$r_{\text{DR,dosSantos}} = -1.1 \times 10^{-7} \times (T/300)^{-0.52} \quad (2)$$

Deviations from the original fit in this temperature range are below $\sim 20\%$.

The situation gets even more complicated when one considers the dependence of the DR rate on the nuclear spin of H_3^+ . The calculations of dos Santos et al. (2007) predict that at $T < 100\text{ K}$ the DR rate is dominated by the *para*- H_3^+ states and at 10 K the rate for $(1,0)$ - H_3^+ is more than an order of magnitude lower than for $(1,1)$ - H_3^+ . These theoretical values are supported by recent afterglow results that see a similar trend (Varju et al. 2011). It should be kept in mind, though, that the calculated rate coefficient at these temperatures depends on the precise position of Rydberg resonances that are difficult to predict, and the initial calculations actually showed the opposite trend (Kokoouline & Greene 2003b).

The first measurements that showed a nuclear spin dependence of the H_3^+ DR rate were carried out at the TSR (Kreckel et al. 2005), however, only a slight enhancement of the rate for *para*- H_3^+ was seen. The same trend has been observed in more recent studies by Tom et al. (2009) and Kreckel et al. (2010). The caveat of these measurements is again the fact that the ions were probably not in their rotational ground states. More detailed studies with state-selected molecular ions are clearly desirable for this important reaction. For now, we implement both extremes in our model calculations, the almost exclusive dominance of the low-energy DR by *para*- H_3^+ , as predicted by the calculations of dos Santos et al. (2007), and basically equal rate coefficients for *ortho*- and *para*- H_3^+ , as seen in the storage ring measurements.

3.3. Dominant pathways

First, to ease our detailed analysis of the chemical processes relevant for the evolution of H_2 and H_3^+ spin states, we identify the dominant pathways in their chemistry. For that we reduce our initially huge gas-grain chemical network with surface reaction to a much smaller set of reactions using our “Automatic Reduction Technique” (ART) tool (see, e.g., Semenov et al. 2006). The reduced network consists of only 20 species and 144 reactions, and is accurate within $< 10\%$ in the studied parameter space for the abundances of H_2 and H_3^+ (see Table 2).

The dominant pathways include ionization by CR particles and UV photons as well as DR and ion-molecule reactions. In comparison to Crabtree et al. (2011), who considered a much simpler chemistry, we find additional pathways that, when combined, bear a significant effect on the resulting *para*-fraction values. Because of the importance that H^+ plays for the H_2 *ortho*-*para* ratios, it becomes necessary to consider the photodissociation of H_2^+ , a major formation pathway of H^+ . Equally important are the DR of the simple molecular ions made of H, C, O, which affects the rate of the H_3^+ DR reaction. We also find that, with the exception being S, elements heavier than oxygen do not have any impact on the hydrogen chemistry. We note that S^+ does not bear any large significance in comparison to C^+ for determining the time-dependent *ortho*-*para* abundances of H_2 and H_3^+ and the effect on the total degree of ionization is at most $\sim 10\%$.

Much as Crabtree et al. (2011), we find that surface processes do not play a significant role in the chemistry of H_2 and H_3^+ . This is because we begin our chemical simulations with hydrogen already being essentially in molecular form and the densities being too low for any efficient surface chemistry to take place. The gas-phase formation of H_2 proceeds via slow neutral-neutral collisions of H atoms or ion-

molecule reactions like $\text{H}_3^+ + \text{O} \rightarrow \text{OH}^+ + \text{H}_2$, and is not efficient.

Aside from DR reactions, there is a small number of ion-molecule reactions that aid in the removal of H_3^+ . The two most notable of the less effective destruction pathways is H_3^+ reacting with OH or O, forming H_2O^+ or OH^+ , respectively, and H_2 . As we show below, at gas hydrogen density of $\sim 10 \text{ cm}^{-3}$ these reactions can slow down the increase in p_3 and causing small changes to occur with time.

Furthermore, we found inconsistencies in the main public astrochemical networks related to the reaction rates of the photodissociation of H_3^+ . Because H_3^+ is expected to be in the ground state in the diffuse interstellar medium, a photon with an energy of almost 20 eV is required for it to be photo-dissociated (Talbi & Saxon 1988). This essentially means that H_3^+ photodissociation is inactive under ISM conditions. Theoretical modeling agrees with this (see e.g. van Dishoeck 1987; van Dishoeck et al. 2006). In the UMIST database (latest version UMIST 2012; McElroy et al. 2013), the correct photodissociation rates for H_3^+ are incorporated. However, this rate is seven orders of magnitude higher in other databases, such as KIDA⁶ and OSU⁷. Because our network is based on the recent osu.2009 network, it had an incorrect rate for the H_3^+ photodissociation on the order of $\sim 10^{-8} \text{ s}^{-1}$, which we have corrected in this study by adopting the corrected value of $5 \times 10^{-15} \text{ s}^{-1}$ from van Dishoeck (1987).

4. Results

4.1. Parameter effects

Implementation of the chemical processes as well as properties of the environment, including density, temperature, and the choice of the chemical age, are the major actors for chemical kinetics modeling. Among these factors, we find that the adopted values of the DR rates have the greatest effect on modeled abundances of *ortho*- and *para*- H_3^+ , while the chemical age, the density, and the CR ionization rate are less important. In our models the *ortho-para* chemistry for H_2 is already at a quasi steady-state after $\sim 10^5$ years, which is shorter than our standard adopted chemical age of $\sim 10^6$ years. Hence, unless otherwise specified, we discuss only the time-dependent evolution of the H_3^+ *ortho-para* chemistry. We calculated the "S" model using two initial abundances with "high" and "low" metal abundances, and found that there is a $< 10\%$ difference in abundances of key molecules. Considering an initially ionized medium (except for H, He, O, N) only shortens the time needed for *para*-fractions to reach their equilibrium values. More importantly, in both these cases, p_2 and p_3 remain unaffected and hence our conclusions are not affected by the choice of initial abundances beyond times $\gtrsim 10^6$ years.

In Figure 2 we show the resulting p_3 and p_2 values for our models with varying density (models "N100" and "N1000"), CR ionization rate (models "C17" and "C15"), time (model "T") and reaction rates for the H_3^+ DR reactions (model "D"), compared to the "Standard" model (model "S").

⁶<http://kida.obs.u-bordeaux1.fr/>

⁷<http://www.physics.ohio-state.edu/~eric/research.html>

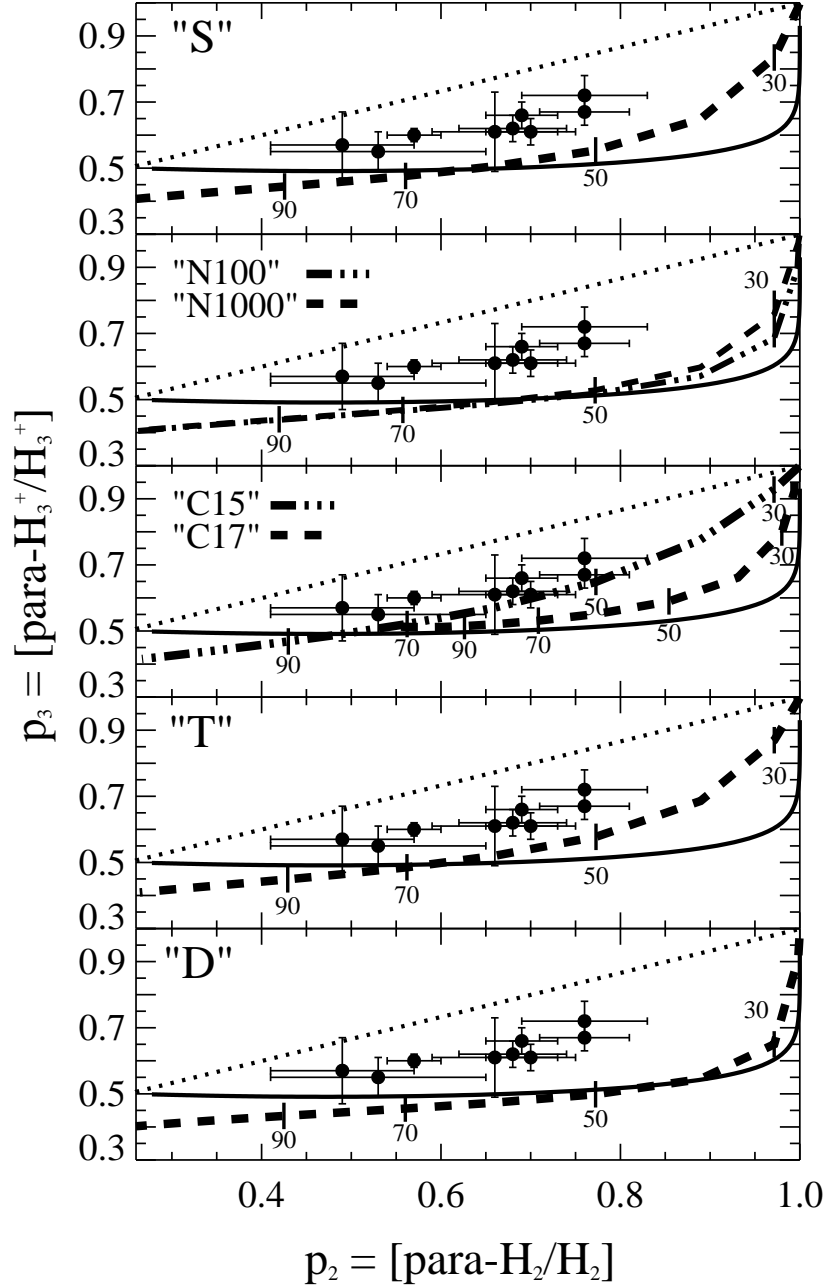


Fig. 2.— Comparison of the effects on p_3 and p_2 values from density, CR ionization rate, time and DR reaction rates compared between our different models, calculated for kinetic temperatures 10 - 100 K. The dotted line is the nascent distribution and solid line the thermal distribution. The calculated p_2 and p_3 values at temperatures 30, 50, 70 and 90 K are marked specifically in the figures. Observation are shown with 1σ error bars. The "S" model is the standard model with $n_H = 10 \text{ cm}^{-3}$, $\zeta_{CR} = 10^{-16} \text{ s}^{-1}$, $A_V = 0.5 \text{ mag}$, adopting the H_3^+ DR rates of McCall et al. (2004) and calculated for temperatures 10–100 K. Compared to the "S" model, in the "N100" and "N1000" models we have increased the hydrogen gas density to $n_H = 100$ and 1000 cm^{-3} respectively, in the "C15" and "C17" models the CR ionization are set to $\zeta_{CR} = 10^{-15}$ and 10^{-17} s^{-1} respectively, in the "T" model the time scale is increased to 10^7 years and in the "D" model the H_3^+ DR rate is set equal to that predicted by dos Santos et al. (2007).

The “S” model does not agree with the trend observed towards diffuse clouds (see Figure 2), but is very similar to the distribution calculated by Crabtree et al. (2011) (see their Figure 8), where they considered only the H_3^+ formation and its destruction by DR. Our models are also compared to thermalized distributions, calculated using energy levels from Lindsay & McCall (2001). The nascent distribution, where $p_3 = 1/3 + 2/3p_2$ is also plotted. For this distribution we assume that H_3^+ is exclusively formed from reaction $\text{H}_2^+ + \text{H}_2$ and we use the branching ratios adopted from nuclear spin selection rules of Quack (1977) and Oka (2004). Furthermore, we assume that the CR ionization of H_2 does not affect the H_2^+ nuclear spin configuration.

We consider three CR ionization rates, 10^{-17} , 10^{-16} and 10^{-15} s^{-1} (models “S”, “C17” and “C15” respectively). The “C17” model decreases the p_3 values while increasing p_2 values, worsening the agreement compared to the “S” model. Meanwhile, the “C15” model significantly improves the fit such that predicted *para*-fractions go through the observed data points. Variations in the CR ionization rate affects the ionization degree, affecting the abundances and *para*-fractions of ions.

Although the diffuse interstellar clouds are likely clumpy, they are often assumed to be homogeneous in astrochemical models. We consider three gas densities typical of diffuse ISM, 10, 100 and 1000 cm^{-3} (model “S”, “N100” and “N1000” respectively). We find that results for model “S” with a hydrogen density of 10 cm^{-3} are closer to the observed values of p_3 . The reason for the higher *para*- H_3^+ fraction with lower density is again the ionization degree of the medium, which is largely determined by H^+ and C^+ . At lower densities the neutralization of the medium through DR reactions proceeds slower, causing a higher ionization degree, however it is not enough to affect the p_2 value.

While we can not predict column densities as our models have no spatial dimension, we can compare the ratios of calculated H_3^+/H_2 abundances to the observed column densities, which should agree unless extreme clumpiness occurs. Doing this, for the final abundances at 1 Myr, our models predicts for temperatures 30 – 70 K abundances ratios $\text{H}_3^+/\text{H}_2 = 2.13 - 8.70 \times 10^{-7}$ for 10 cm^{-3} (model “S”), $1.12 - 2.34 \times 10^{-7}$ for 100 cm^{-3} (model “N100”) and $2.37 - 4.77 \times 10^{-8}$ for 1000 cm^{-3} (model “N1000”), while observed column density ratios are typically $\sim 10^{-7}$ (Crabtree et al. 2011; Indriolo & McCall 2012, and this study). This means that modeled abundances for the gas density 100 cm^{-3} agree better with the observed H_3^+/H_2 ratios, while the p_3 values still disagree. It also becomes clear that the temperature has a larger effect on abundances at 10 cm^{-3} than at 100 cm^{-3} , considering the predicted wide range of abundances for the 10 cm^{-3} model. The effects of the CR ionization modeled in the “C17” and “C15” models also affects the H_3^+/H_2 abundances ratios, and for the former we calculate $\text{H}_3^+/\text{H}_2 = 1.30 - 2.10 \times 10^{-7}$ and for the latter $\text{H}_3^+/\text{H}_2 = 6.25 - 7.75 \times 10^{-7}$. This means that the “C15” model improves the agreement in the *para*-fraction distributions and the calculated H_3^+/H_2 abundance ratios are within reasonable agreement to observed column densities.

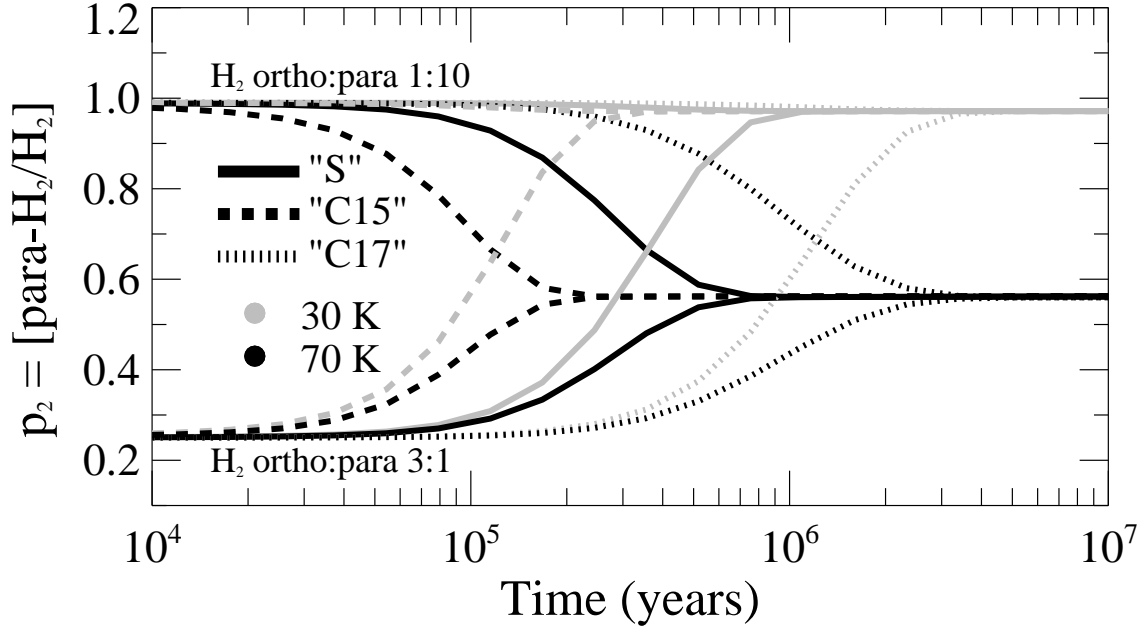


Fig. 3.— Evolution of p_2 with time. Results from the “S” model are shown by the solid line, the “C17” model by dashed line and the “C15” model by dot-dashed line. Two different initial H_2 *ortho:para* are tested: 1:10 and 3:1. H_2 para-fractions at 30 K are shown in gray and in black 70 K.

4.1.1. Time-dependence

In Figure 3 we show the evolution of p_2 values for models “S”, “C15” and “C17” as a function of time for two separate temperatures, 30 K and 70 K, and considering two initial H_2 *ortho/para* ratio, 3:1 (equilibrium ratio) and 1:10 (ratio of colder environments). At 30 K the p_2 values do not change significantly between models “S”, “C15” and “C17”, as they are close to the thermalized value already from the beginning. The “S” model reaches its 30 K steady-state value $p_2 \approx 0.97$ after $\sim 10^6$ years, while the 70 K value $p_2 \approx 0.56$ requires only $\sim 7 \times 10^5$ years. However, in the “C17” model it takes longer, $\sim 3 \times 10^6$ years at both 30 and 70 K, to reach the same steady-state values, as opposed to $\sim 2 \times 10^5$ years for the “C15” model. This means that the results are strongly time-dependent, and the steady-state p_2 values have not changed, but merely the process of reaching the steady-state values is slowed down. The variation in CR ionization rate affects the production of H^+ , the essential thermalization agent of H_2 and this further affects the time it takes to reach the thermalized *ortho/para* ratio. The calculated *para*-fractions become independent of the modeling assumptions on time scales $\gtrsim 10^7 - 10^8$ years.

Contrary to the H_2 evolution, the modeled *ortho-para* H_3^+ abundances have not reached steady-state by the chemical age of 10^6 years. Therefore, we study how p_3 evolves in the “S” model at later times up to 10^7 years (model “T”, see Figure 2). In general, the p_3 values increase with temperature and the temperature distribution slowly approaches the nascent distribution. However, this process appears to require an unrealistic amount of time exceeding 10^8 years for models “N100” and “N1000”. It is clear that even

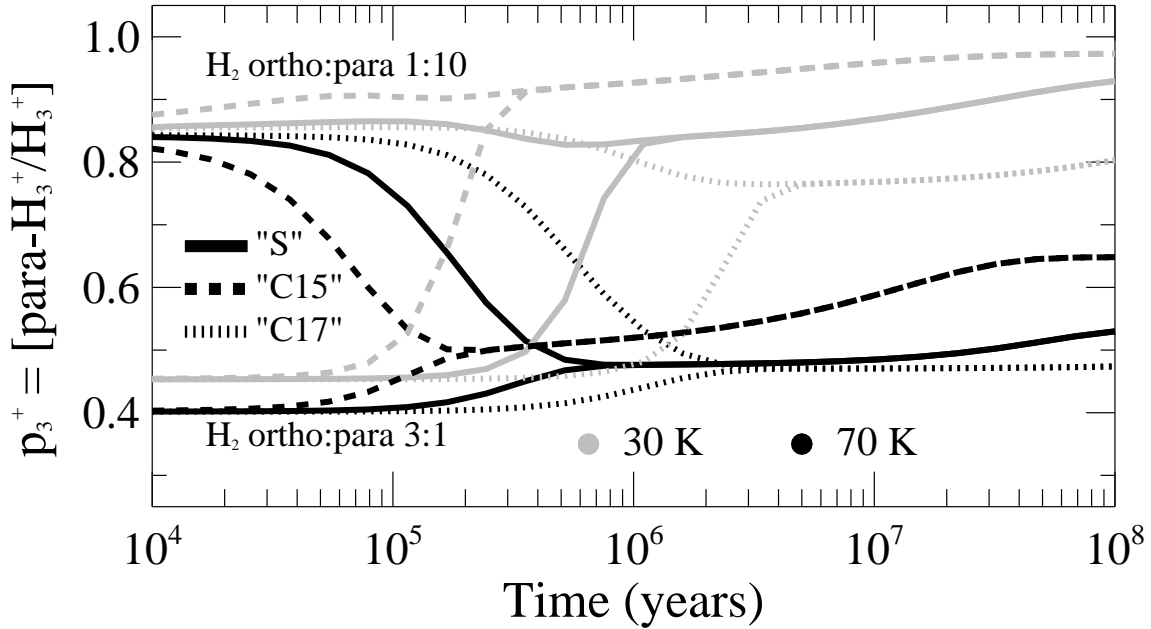


Fig. 4.— Evolution of p_2 with time. Results from the “S” model are shown by the solid line, the “C17” model by dashed line and the “C15” model by dot-dashed line. Two different initial H_2 *ortho:para* are tested: 1:10 and 3:1. H_2 para-fractions at 30 K are shown in gray and in black 70 K.

after only $\sim 10^7$ years the p_3 distribution is showing an appreciable difference to its value after 10^6 years.

This becomes much clearer in Figure 4 where the time evolution of p_3 is shown for the “S”, “C15” and “C17” models up to 10^8 years. We can see that 10^8 years are necessary in order for the “C15” model to reach steady-state while the other models needs even longer time scales as the p_3 values are slowly increasing with time until they reach steady-state values of $p_3 \approx 0.97$ at 30 K and $p_3 \approx 0.67$ at 70 K. This steady increase in p_3 values is due to the slow redistribution of hydrogen from molecular into atomic form (H and H^+). We can conclude that it is clear that steady-state models are not appropriate in modeling the p_3 values of diffuse clouds.

4.1.2. Influence of DR rate coefficient

The total rate and branching ratios for the DR of (1,0)– and (1,1)– H_3^+ greatly affects the modeled p_3 values (see Figure 2). In model “D” we compare the p -values of H_3^+ and H_2 for the chemical models adopting a branching ratio of $\sim 1:15$ for the *ortho:para* H_3^+ DR rates, as predicted by dos Santos et al. (2007). There are clear differences between the various models and the observed values, with the largest discrepancy arising at temperatures $\lesssim 60$ K, which are typical representative temperatures of the diffuse ISM (Snow & McCall 2006). The H_3^+ DR process with a preferred destruction of (1,1)– H_3^+ results in p_3 values that are lower than the thermalized distribution at temperatures > 30 K. The p_3 values continue to decrease

with time. As we adjust the DR branching ratio for (1,0)– and (1,1)– H_3^+ towards unity, the overall p_3 values increase, most notably at low temperatures, and approximately at a ratio of 1 : 5 the time dependence is reversed, and the p_3 values begin to slowly increase with time. The key conclusion is that while the total DR rate coefficient does not play a significant role as long as the branching ratio is $\lesssim 1:5$, a DR branching ratio approaching unity for (1, 1)– and (1, 0)– H_3^+ is necessary in order to reproduce the observed distributions. Furthermore, the H_3^+/H_2 ratios in the “D” model are not significantly affected by variations in the DR branching ratio, the H_3^+/H_2 values are similar to those predicted for the “S” model.

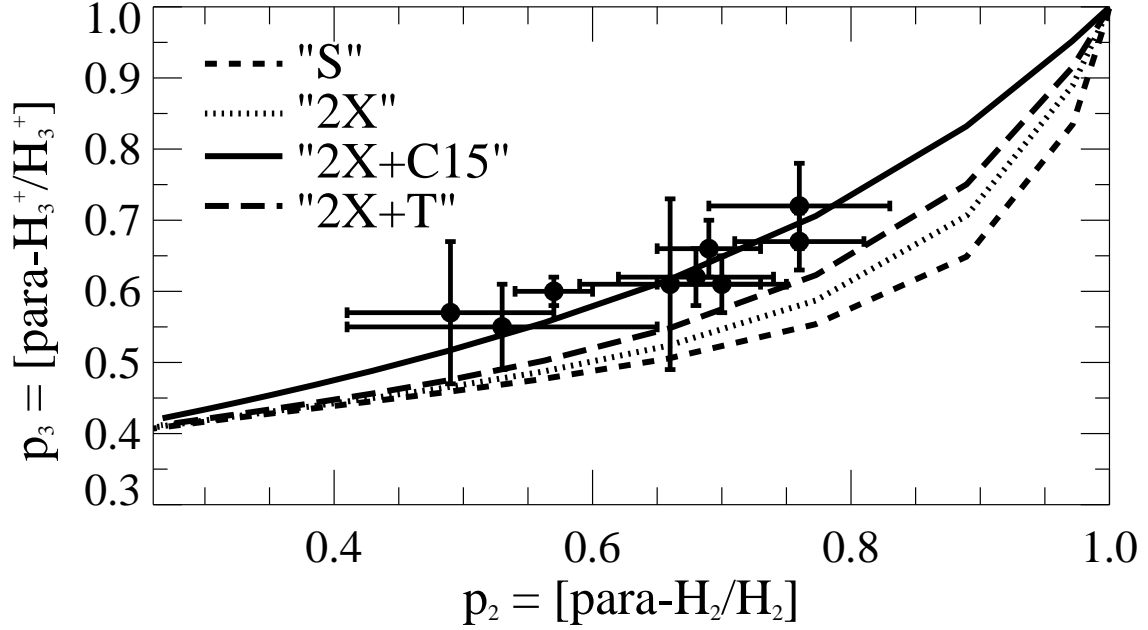


Fig. 5.— The p_3 and p_2 values calculated with the standard chemical model for 1 Myr (dashed line) for temperatures of 10 - 100 K, with variations in the total DR reaction rates. DR rates are increased by a factor of 2 (dotted line, model “2X”) and also combined with an increase in chemical age to 10^7 years (long dashed line, model “2X+T”) and an increase CR rate to 10^{-15} s^{-1} (solid line, model “2X+C15”). Observations are shown with error bars.

It is clear that the increased DR rate of *ortho*- H_3^+ improves the fit to observations, but the question remains if a higher total DR rate can also affect results, while the relative rate between (1, 1)– and (1, 0)– H_3^+ remains the same. In Figure 5 we compare the results of increasing the total DR rate in the “S” model by a factor 2 (dotted line, model “2X”) which significantly improves the fit. Because the p_3 value is largely determined by the ratio between thermalization and DR processes, an increase in the DR rate can also be considered the same effect as if the thermalization process is slowed down, as was discussed by Crabtree et al. (2011) (see their Figure 6).

4.2. Best-fit model

A high total DR rate will cause the time effect to be more significant, hence we have also calculated a model at 10^7 years. The additional longer time scale improves our fit and we find that the resulting distribution of *para*-fractions is similar to what is predicted in the “2X” model. Furthermore, the total H_3^+ abundance decreases further, and at 10^7 years $\text{H}_3^+/\text{H}_2 = (1.41 - 2.62) \times 10^{-7}$, which is closer to the observed values.

Because the H_3^+ abundance is also strongly affected, the H_3^+/H_2 ratio decreases by a similar factor of ~ 2 and ~ 4 for the same increase in the total DR rate, respectively. The H_3^+/H_2 ratio drops to values similar to the observed values of $\sim 10^{-7}$. It means that an increased total DR rate also has the added benefit of improving the agreement to the calculations of the H_3^+ column densities. By combining the effects of an increased DR rate and increased chemical age (model “2X + T”) we achieve a p_3 distribution that is approaching the observed distribution and where $\text{H}_3^+/\text{H}_2 = 1.73 - 3.94 \times 10^{-7}$ is largely similar to the observed column densities.

A higher CR ionization rate (model “C15” with $\zeta_{CR} = 10^{-15} \text{ s}^{-1}$) was shown to have a positive effect on improving the fit to observations. Combining the effect of the increased DR rate with an increased CR ionization rate (“2X + C15”) further helps to improve the agreement with observations. We find that the best fit to observations is achieved with the “2X + C15” model where predicted p_2 and p_3 values clearly go through the observation data points. The calculated $\text{H}_3^+/\text{H}_2 = 4.61 - 7.62 \times 10^{-7}$ is somewhat higher due to the increased CR ionization rate, but similar to that predicted for the “C15” model.

4.3. Other molecules

While we have been concentrating on the abundances of H_3^+ and H_2 , other molecules have also been observed in diffuse clouds and will be affected by the variations of model parameters. In Figure 6 the range of calculated abundances from the models in Table 2 are compared to a compilation of observations in diffuse clouds from Snow & McCall (2006).

The calculated abundances cover a wide range that shows an agreement with several observed molecules (grey lines), especially CH, CO, OH, H_2 , H_3^+ and HD. Amongst the molecules difficult to fit we find molecules such as CH^+ , HCN, HNC, HCO^+ . If we consider only the best-fit model “2X+C15” we see that we underpredict abundances by many orders of magnitude (see gray lines of Figure 6), however the calculated H_3^+ abundances at ~ 50 K are in agreement with observed values.

HCl shows a underprediction of abundances by approximately 2 orders of magnitude compared to observations, likely due to the very limited Cl-based chemistry in our network which makes our predicted HCl abundances very uncertain.

Although CH^+ is a simple ion, it has for long been recognised as a problematic molecule to explain in the diffuse ISM (see e.g. Duley et al. 1992; Federman et al. 1996; Pan & Padoan 2009). Its expected slow

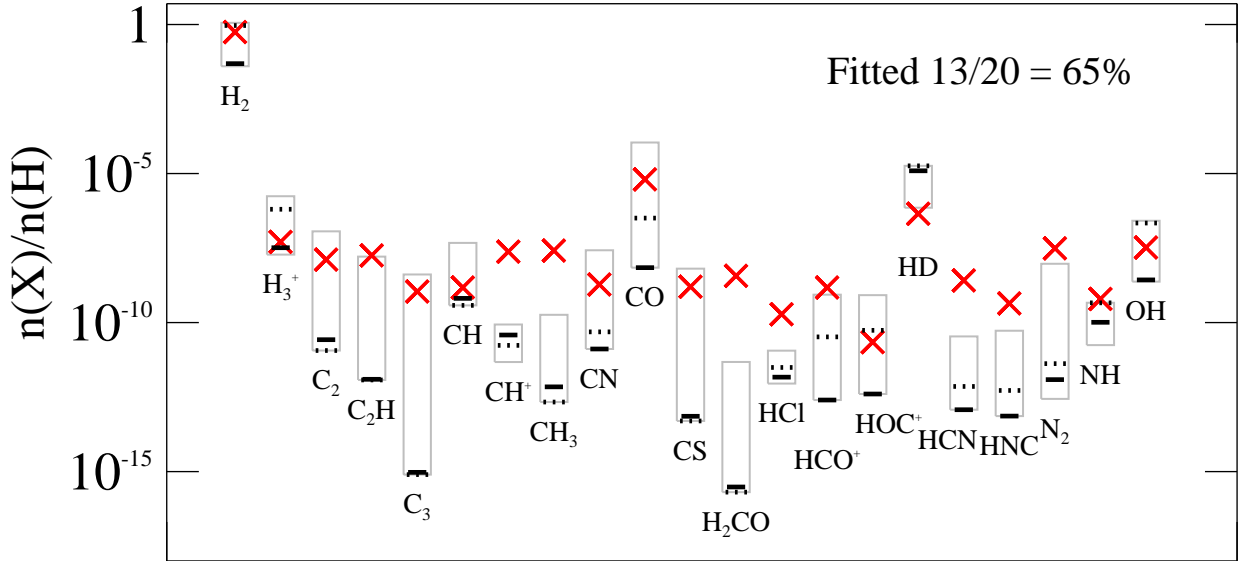


Fig. 6.— Comparison of observed abundances (red crosses) to modeled values of key species in diffuse clouds. Gray boxes show the range of abundances calculated from the considered models (Table 2) and black lines show abundances from the best-fit model “2X+C15” (30 K, solid line, and 90 K, dotted line). A colored version of the figure is available in the online version of the paper.

formation through radiative association mechanism $C^+ + H \rightarrow CH^+ + h\nu$ or $C^+ + H_2 \rightarrow CH_2^+$ followed by photodissociation while being rapidly destroyed through reactions with H, H_2 and e^- is causing models to underpredict abundances by two orders of magnitude compared to observations. A possible solution to explain this discrepancy is finding a physical processes that would allow the endothermic reaction $C^+ + H_2 \rightarrow CH^+ + H$ to be effective and drive the production of CH^+ , such as shocks or turbulence (see e.g. Draine & Katz 1986; Falgarone et al. 2005).

In the diffuse ISM, lacking efficient surface chemistry, H_2CO is formed through the reaction $CH_3 + O \rightarrow H_2CO + H$. The underproduction of H_2CO should therefore be able to be traced through the CH_3 formation, which begins with CH^+ and the subsequent formation of CH_2^+ and CH_3^+ through hydrogenation by reacting with H_2 . As we can see from Figure 6, CH^+ is similarly underproduced as CH_3 and H_2CO , and it is likely that the underproduction is related to that of CH^+ , which is mainly formed through H_3^+ reacting with C atoms. Since we can show a good agreement to H_3^+ observations, we can conclude that C atoms must be underproduced in chemical models. However, because atomic C has not been observed, this can not be tested.

For species such as HCN, HNC and N_2 , light hydrocarbons first need to be formed, making these species late-time and hence strongly dependent on the chemical age and calculated abundances are very uncertain.

The abundances of these species may also be affected by other processes and parameters such as the clumpiness of the environments, initial abundances and the chemistry of molecules in excited states (see e.g.

Spaans 1996; Price et al. 2003; Bethell et al. 2007; Agúndez et al. 2010; Oka 2013; Agúndez & Wakelam 2013).

5. Conclusions

We present the results of three new sight lines towards diffuse clouds, where both H_3^+ and H_2 have been observed in their *ortho* and *para* forms. The new observations follow the same trend as found by Crabtree et al. (2011), lying between the nascent and thermalized distribution. We come to the conclusion that H_3^+ is not fully thermalized as the thermalization by collisions with H_2 is competing with destruction of H_3^+ by dissociative recombination.

To study this, we conducted the first time-dependent modeling of the nuclear spin-states of H_2 and H_3^+ in the diffuse interstellar medium, and compared our results to the observed values, including the new measurements.

We found that the DR of H_3^+ is a key process that governs the p_3 values. Our model indicates that a branching ratio of ~ 1 between the (1, 1)- and (1, 0)- H_3^+ dissociation is needed to achieve an agreement with the observations. An increased CR ionization rate to 10^{-15} s^{-1} also has a significant effect on the p_3 values and brings the calculated values much closer to the observed values. The remaining studied parameters, initial H_2 *ortho/para* ratio, n_H , chemical age and total DR rates will increase the pace at which the p_3 values approach the nascent distribution by a smaller, but significant amount.

However, increasing the CR ionization rate to 10^{-15} s^{-1} causes difficulties with reproducing observed abundances of other molecules, whereas many molecules are underproduced by our models. This is the same problem that has been raised before in the discussion of H_3^+ in diffuse clouds, but here we can also show that the high CR ionization rate is an essential ingredient in order to achieve an agreement with the *para*-fractions of H_3^+ .

We conclude that the best fit to observations is achieved for the “2X+C15” model with a density of 10 cm^{-3} , CR ionization rate 10^{-15} s^{-1} , a 1:1 DR branching ratio, a time scale of 10^6 years and a total DR rate a factor of 2 larger than that derived by (McCall et al. 2004), or an equivalent reduction of thermalization rates (see Figure 6 of Crabtree et al. 2011). With this model, we find that our predicted H_3^+/H_2 values match that derived from the observed column densities within an order of magnitude (where the largest impact is due to the adopted density and CR ionization rate).

These results warrant a more detailed study with a better treatment of the clumpy structure of diffuse clouds. Furthermore, better understanding of the CR ionization rate, and its possible variation within the diffuse cloud, and chemical ages need to be better constrained for future studies (e.g. Rimmer et al. 2012). It is also evident that the H_3^+ DR process is vital in order to better understand the *ortho–para* hydrogen chemistry in the diffuse ISM. For that, one has to bring in agreement the laboratory results on the DR of H_3^+ obtained with various experimental setups, such as the storage ring experiments (Kreckel et al. 2005; Tom et al. 2009; Kreckel et al. 2010), and the afterglow experiments (e.g. Gougousi et al. 1995; Laubé et al.

1998; Plašil et al. 2002; Glosík et al. 2009). Therefore, we highly recommend new accurate studies of the H_3^+ DR reactions, in order to both determine the absolute DR rate as well as the nuclear spin dependence for the lowest rotational states.

We would like to thank the anonymous referee for their useful comments that helped improve this paper. This research made use of NASA’s Astrophysics Data System. TA acknowledges funding from the European Community’s Seventh Framework Programme [FP7/2007-2013] under grant agreement no. 238258. N.I. is funded by NASA Research Support Agreement No. 1465490 provided through JPL. H.K. was supported by the European Research Council under Grant Agreement No. StG 307163. DS acknowledges support by the *Deutsche Forschungsgemeinschaft* through SPP 1385: “The first ten million years of the Solar System - a planetary materials approach” (SE 1962/1-3). KNC has been supported by a CfA Postdoctoral Fellowship from the Smithsonian Astrophysical Observatory.

Table 3. The dominant reactions for the hydrogen chemistry in the diffuse ISM. Values in parenthesis are exponential factors. Errors are defined as values for a log-normal distribution, with standard deviation $k \pm$ error. Errors marked with an asterisk (*) are resulting from our separation scheme to generate *ortho-para* reactions, and uncertainties are taken from the original reaction, but are likely higher.

Reaction	α	β	γ	Error
H + CR → H ⁺ + e ⁻	0.46	0	0	2.00
oH ₂ + CR → H ⁺ + H + e ⁻	0.02	0	0	2.00*
pH ₂ + CR → H ⁺ + H + e ⁻	0.02	0	0	2.00*
oH ₂ + CR → oH ₂ ⁺ + e ⁻	0.93	0	0	2.00*
pH ₂ + CR → pH ₂ ⁺ + e ⁻	0.93	0	0	2.00*
oH ₂ + CR → 2H	0.10	0	0	2.00*
pH ₂ + CR → 2H	0.10	0	0	2.00*
He + CR → He ⁺ + e ⁻	0.50	0	0	2.00
C + CR → C ⁺ + e ⁻	1.02(3)	0	0	2.00
O + CR → O ⁺ + e ⁻	2.80	0	0	2.00
S + hν _{CR} → S ⁺ + e ⁻	9.60(2)	0	0	2.00
OH + hν _{CR} → O + H	5.10(2)	0	0	2.00
C + hν _{CR} → C ⁺ + e ⁻	1.02(3)	0	0	2.00
H + hν _{CR} → H ⁺ + e ⁻	0.46	0	0	2.00
He + hν _{CR} → He ⁺ + e ⁻	0.50	0	0	2.00
O + hν _{CR} → O ⁺ + e ⁻	2.80	0	0	2.00
oH ₂ + hν _{CR} → 2H	0.10	0	0	2.00*
pH ₂ + hν _{CR} → 2H	0.10	0	0	2.00*
oH ₂ + hν _{CR} → H ⁺ + H + e ⁻	0.02	0	0	2.00*
pH ₂ + hν _{CR} → H ⁺ + H + e ⁻	0.02	0	0	2.00*
oH ₂ + hν _{CR} → oH ₂ ⁺ + e ⁻	0.93	0	0	2.00*
pH ₂ + hν _{CR} → pH ₂ ⁺ + e ⁻	0.93	0	0	2.00*
C + UV → C ⁺ + e ⁻	0.22(-9)	0	2.61	2.00
OH + UV → OH ⁺ + e ⁻	0.16(-11)	0	3.10	2.00
OH + UV → O + H	0.17(-9)	0	1.66	2.00
OH ⁺ + UV → H ⁺ + O	0.72(-11)	0	1.80	2.00
S + UV → S ⁺ + e ⁻	0.72(-9)	0	2.40	2.00
oH ₂ + UV → 2H	0.34(-10)	0	2.50	2.00*
pH ₂ + UV → 2H	0.34(-10)	0	2.50	2.00*
oH ₂ ⁺ + UV → H ⁺ + H	0.26(-9)	0	1.80	2.00*
pH ₂ ⁺ + UV → H ⁺ + H	0.26(-9)	0	1.80	2.00*
C ⁺ + S → S ⁺ + C	0.15(-8)	0	0	2.00
H ⁺ + O → O ⁺ + H	0.70(-9)	0	2.32(2)	1.50
H ⁺ + OH → OH ⁺ + H	0.16(-7)	-0.50	0	2.00
H ⁺ + S → S ⁺ + H	0.13(-8)	0	0	2.00
oH ₂ ⁺ + H → H ⁺ + oH ₂	0.64(-9)	0	0	1.25*
pH ₂ ⁺ + H → H ⁺ + pH ₂	0.64(-9)	0	0	1.25*
pH ₂ ⁺ + oH ₂ → pH ₃ ⁺ + H	0.14(-8)	0	0	2.00

Table 3—Continued

Reaction	α	β	γ	Error
$\text{oH}_2^+ + \text{O} \rightarrow \text{OH}^+ + \text{H}$	0.15(–8)	0	0	2.00*
$\text{pH}_2^+ + \text{O} \rightarrow \text{OH}^+ + \text{H}$	0.15(–8)	0	0	2.00*
$\text{oH}_2^+ + \text{OH} \rightarrow \text{H}_2\text{O}^+ + \text{H}$	0.76(–9)	0	0	2.00*
$\text{pH}_2^+ + \text{OH} \rightarrow \text{H}_2\text{O}^+ + \text{H}$	0.76(–9)	0	0	2.00*
$\text{oH}_2^+ + \text{OH} \rightarrow \text{OH}^+ + \text{oH}_2$	0.76(–9)	0	0	2.00*
$\text{pH}_2^+ + \text{OH} \rightarrow \text{OH}^+ + \text{pH}_2$	0.76(–9)	0	0	2.00*
$\text{oH}_3^+ + \text{O} \rightarrow \text{OH}^+ + \text{oH}_2$	0.80(–9)	–0.16	1.41	1.41*
$\text{pH}_3^+ + \text{O} \rightarrow \text{OH}^+ + \text{oH}_2$	0.40(–9)	–0.16	1.41	1.41*
$\text{pH}_3^+ + \text{O} \rightarrow \text{OH}^+ + \text{pH}_2$	0.40(–9)	–0.16	1.41	1.41*
$\text{oH}_3^+ + \text{OH} \rightarrow \text{H}_2\text{O}^+ + \text{oH}_2$	0.95(–8)	–0.50	0	2.00*
$\text{pH}_3^+ + \text{OH} \rightarrow \text{H}_2\text{O}^+ + \text{oH}_2$	0.47(–8)	–0.50	0	2.00*
$\text{pH}_3^+ + \text{OH} \rightarrow \text{H}_2\text{O}^+ + \text{pH}_2$	0.47(–8)	–0.50	0	2.00*
$\text{He}^+ + \text{H} \rightarrow \text{H}^+ + \text{He}$	0.19(–14)	0	0	1.25
$\text{He}^+ + \text{oH}_2 \rightarrow \text{oH}_2^+ + \text{He}$	0.96(–14)	0	0	2.00*
$\text{He}^+ + \text{pH}_2 \rightarrow \text{oH}_2^+ + \text{He}$	0.64(–14)	0	0	2.00*
$\text{He}^+ + \text{pH}_2 \rightarrow \text{pH}_2^+ + \text{He}$	0.32(–14)	0	0	2.00*
$\text{He}^+ + \text{oH}_2 \rightarrow \text{H}^+ + \text{H} + \text{He}$	0.11(–12)	–0.24	0	2.00*
$\text{He}^+ + \text{pH}_2 \rightarrow \text{H}^+ + \text{H} + \text{He}$	0.11(–12)	–0.24	0	2.00*
$\text{He}^+ + \text{OH} \rightarrow \text{O}^+ + \text{H} + \text{He}$	0.85(–8)	–0.50	0	2.00
$\text{O}^+ + \text{H} \rightarrow \text{H}^+ + \text{O}$	0.70(–9)	0	0	1.50
$\text{O}^+ + \text{oH}_2 \rightarrow \text{OH}^+ + \text{H}$	0.16(–8)	0	0	1.25*
$\text{O}^+ + \text{pH}_2 \rightarrow \text{OH}^+ + \text{H}$	0.16(–8)	0	0	1.25*
$\text{O}^+ + \text{OH} \rightarrow \text{OH}^+ + \text{O}$	0.36(–9)	0	0	2.00
$\text{OH}^+ + \text{oH}_2 \rightarrow \text{H}_2\text{O}^+ + \text{H}$	0.11(–8)	0	0	1.25*
$\text{OH}^+ + \text{pH}_2 \rightarrow \text{H}_2\text{O}^+ + \text{H}$	0.11(–8)	0	0	1.25*
$\text{OH}^+ + \text{OH} \rightarrow \text{H}_2\text{O}^+ + \text{O}$	0.70(–9)	0	0	2.00
$\text{OH}^+ + \text{S} \rightarrow \text{S}^+ + \text{OH}$	0.43(–9)	0	0	2.00
$\text{H}^+ + \text{H} \rightarrow \text{oH}_2^+$	0.20(–19)	1.00	0	2.00*
$\text{H}^+ + \text{H} \rightarrow \text{pH}_2^+$	0.20(–19)	1.00	0	2.00*
$\text{H} + \text{OH} \rightarrow \text{O} + \text{oH}_2$	0.69(–13)	2.80	1.70(2)	2.00*
$\text{H} + \text{OH} \rightarrow \text{O} + \text{pH}_2$	0.69(–13)	2.80	1.95(3)	2.00*
$\text{oH}_2 + \text{O} \rightarrow \text{OH} + \text{H}$	0.34(–12)	2.67	3.16(3)	3.16*
$\text{pH}_2 + \text{O} \rightarrow \text{OH} + \text{H}$	0.34(–12)	2.67	3.16(3)	3.16*
$\text{H} + \text{O} \rightarrow \text{OH}$	0.99(–18)	–0.38	0	10.0
$\text{oH}_2^+ + \text{e}^- \rightarrow 2\text{H}$	0.16(–7)	–0.43	0	2.00*
$\text{pH}_2^+ + \text{e}^- \rightarrow 2\text{H}$	0.16(–7)	–0.43	0	2.00*
$\text{H}_2\text{O}^+ + \text{e}^- \rightarrow \text{OH} + \text{H}$	0.86(–7)	–0.50	0	1.25
$\text{H}_2\text{O}^+ + \text{e}^- \rightarrow \text{O} + \text{H} + \text{H}$	0.30(–6)	–0.50	0	1.25

Table 3—Continued

Reaction	α	β	γ	Error
$\text{H}_2\text{O}^+ + \text{e}^- \rightarrow \text{O} + \text{oH}_2$	0.39(−7)	−0.50	1.70(2)	1.25*
$\text{H}_2\text{O}^+ + \text{e}^- \rightarrow \text{O} + \text{pH}_2$	0.39(−7)	−0.50	0	1.25*
$\text{oH}_3^+ + \text{e}^- \rightarrow \text{oH}_2 + \text{H}$		see Section 3.2.1		
$\text{pH}_3^+ + \text{e}^- \rightarrow \text{oH}_2 + \text{H}$		see Section 3.2.1		
$\text{pH}_3^+ + \text{e}^- \rightarrow \text{pH}_2 + \text{H}$		see Section 3.2.1		
$\text{oH}_3^+ + \text{e}^- \rightarrow 3\text{H}$		see Section 3.2.1		
$\text{pH}_3^+ + \text{e}^- \rightarrow 3\text{H}$		see Section 3.2.1		
$\text{OH}^+ + \text{e}^- \rightarrow \text{O} + \text{H}$	0.63(−8)	−0.48	0	1.25
$\text{C}^+ + \text{e}^- \rightarrow \text{C}$	0.44(−11)	−0.61	0	1.50
$\text{H}^+ + \text{e}^- \rightarrow \text{H}$	0.35(−11)	−0.70	0	2.00
$\text{He}^+ + \text{e}^- \rightarrow \text{He}$	0.45(−11)	−0.67	0	2.00
$\text{O}^+ + \text{e}^- \rightarrow \text{O}$	0.34(−11)	−0.63	0	2.00
$\text{S}^+ + \text{e}^- \rightarrow \text{S}$	0.39(−11)	−0.63	0	2.00
$\text{oH}_3^+ + \text{O} \rightarrow \text{H}_2\text{O}^+ + \text{H}$	0.34(−9)	−0.16	1.41	1.41*
$\text{pH}_3^+ + \text{O} \rightarrow \text{H}_2\text{O}^+ + \text{H}$	0.34(−9)	−0.16	1.41	1.41*
$\text{H} + \text{H} \rightarrow \text{oH}_2$	0.50(−16)	0.50	1.70(2)	2.00*
$\text{H} + \text{H} \rightarrow \text{pH}_2$	0.50(−16)	0.50	0	2.00*
$\text{H}^+ + \text{oH}_2 \rightarrow \text{oH}_2^+ + \text{H}$	0.64(−9)	0	2.13(4)	2.00
$\text{H}^+ + \text{pH}_2 \rightarrow \text{oH}_2^+ + \text{H}$	0.43(−9)	0	2.13(4)	2.00
$\text{H}^+ + \text{pH}_2 \rightarrow \text{pH}_2^+ + \text{H}$	0.21(−9)	0	2.13(4)	2.00
$\text{oH}_3^+ + \text{H} \rightarrow \text{pH}_2^+ + \text{oH}_2$	0.21(−8)	0	2.00(4)	2.00*
$\text{pH}_3^+ + \text{H} \rightarrow \text{pH}_2^+ + \text{oH}_2$	0.10(−8)	0	2.00(4)	2.00*
$\text{pH}_3^+ + \text{H} \rightarrow \text{pH}_2^+ + \text{pH}_2$	0.10(−8)	0	2.00(4)	2.00*
$\text{C}^+ + \text{H} \rightarrow \text{H}^+ + \text{C}$	0.93(−18)	1.30	1.59(4)	2.00
$\text{S}^+ + \text{H} \rightarrow \text{H}^+ + \text{S}$	0.57(−15)	1.20	2.72(4)	2.00
$\text{H}^+ + \text{C} \rightarrow \text{C}^+ + \text{H}$	1.00(−14)	0	0	2.00
$\text{pH}_3^+ + \text{oH}_2 \rightarrow \text{pH}_3^+ + 2\text{H}$	0.30(−10)	0.50	5.20(4)	2.00
$\text{He}^+ + \text{oH}_2 \rightarrow \text{He}^+ + 2\text{H}$	0.30(−10)	0.50	5.20(4)	2.00*

REFERENCES

- Agúndez, M., Goicoechea, J. R., Cernicharo, J., Faure, A., & Roueff, E. 2010, *ApJ*, 713, 662
- Agúndez, M. & Wakelam, V. 2013, *Chemical Reviews*, 113, 8710
- Albertsson, T., Semenov, D. A., Vasyunin, A. I., Henning, T., & Herbst, E. 2013, *ApJS*, 207, 27
- Bethell, T. J., Zweibel, E. G., & Li, P. S. 2007, *ApJ*, 667, 275
- Cardelli, J. A., Meyer, D. M., Jura, M., & Savage, B. D. 1996, *ApJ*, 467, 334
- Caselli, P. 2003, *Ap&SS*, 285, 619
- Cecchi-Pestellini, C., Williams, D. A., Viti, S., & Casu, S. 2009, *ApJ*, 706, 1429
- Chehrouri, M., Fillion, J.-H., Chaabouni, H., et al. 2011, *Physical Chemistry Chemical Physics (Incorporating Faraday Transactions)*, 13, 2172
- Crabtree, K. N., Indriolo, N., Kreckel, H., Tom, B. A., & McCall, B. J. 2011, *ApJ*, 729, 15
- Crabtree, K. N. & McCall, B. J. 2012, *Philosophical Transactions of the Royal Society A: Mathematical, Physical and Engineering Sciences*, 370, 5055
- Crabtree, K. N. & McCall, B. J. 2013, *The Journal of Physical Chemistry A*, 117, 9950
- dos Santos, S. F., Kokoouline, V., & Greene, C. H. 2007, *The Journal of Chemical Physics*, 127, 124309
- Draine, B. T. & Bertoldi, F. 1996, *ApJ*, 468, 269
- Draine, B. T. & Katz, N. 1986, *ApJ*, 310, 392
- Duley, W. W., Hartquist, T. W., Sternberg, A., Wagenblast, R., & Williams, D. A. 1992, *MNRAS*, 255, 463
- Falgarone, E., Godard, B., Pineau des Forêts, G., & Gerin, M. 2013, in *IAU Symposium, Vol. 292, IAU Symposium*, ed. T. Wong & J. Ott, 223–226
- Falgarone, E., Verstraete, L., Pineau Des Forêts, G., & Hily-Blant, P. 2005, *A&A*, 433, 997
- Federman, S. R., Rawlings, J. M. C., Taylor, S. D., & Williams, D. A. 1996, *MNRAS*, 279, L41
- Flower, D. R., Pineau des Forêts, G., & Walmsley, C. M. 2004, *A&A*, 427, 887
- Geballe, T. R., McCall, B. J., Hinkle, K. H., & Oka, T. 1999, *ApJ*, 510, 251
- Geballe, T. R. & Oka, T. 1996, *Nature*, 384, 334
- Gerlich, D. 1990, *J. Chem. Phys.*, 92, 2377
- Gibb, E. L., Brittain, S. D., Rettig, T. W., et al. 2010, *ApJ*, 715, 757

- Glosík, J., Plašil, R., Korolov, I., et al. 2009, *Phys. Rev. A*, 79, 052707
- Goto, M., Usuda, T., Nagata, T., et al. 2008, *ApJ*, 688, 306
- Gougousi, T., Johnsen, R., & Golde, M. F. 1995, *International Journal of Mass Spectrometry and Ion Processes*, 149, 131
- Graedel, T. E., Langer, W. D., & Frerking, M. A. 1982, *ApJS*, 48, 321
- Grussie, F., Berg, M. H., Crabtree, K. N., et al. 2012, *ApJ*, 759, 21
- Honvault, P., Jorfi, M., González-Lezana, T., Faure, A., & Pagani, L. 2011, *Physical Review Letters*, 107, 023201
- Hugo, E., Asvany, O., & Schlemmer, S. 2009, *J. Chem. Phys.*, 130, 164302
- Indriolo, N., Fields, B. D., & McCall, B. J. 2009, *ApJ*, 694, 257
- Indriolo, N., Geballe, T. R., Oka, T., & McCall, B. J. 2007, *ApJ*, 671, 1736
- Indriolo, N. & McCall, B. J. 2012, *ApJ*, 745, 91
- Jenkins, E. B. 2009, *ApJ*, 700, 1299
- Kaeuff, H.-U., Ballester, P., Biereichel, P., et al. 2004, in *Society of Photo-Optical Instrumentation Engineers (SPIE) Conference Series*, Vol. 5492, *Society of Photo-Optical Instrumentation Engineers (SPIE) Conference Series*, ed. A. F. M. Moorwood & M. Iye, 1218–1227
- Kokoouline, V. & Greene, C. H. 2003a, *Physical Review Letters*, 90, 133201
- Kokoouline, V. & Greene, C. H. 2003b, *Phys. Rev. A*, 68, 012703
- Kokoouline, V., Greene, C. H., & Esry, B. D. 2001, *Nature*, 412, 891
- Kreckel, H., Motsch, M., Mikosch, J., et al. 2005, *Physical Review Letters*, 95, 263201
- Kreckel, H., Novotný, O., Crabtree, K. N., et al. 2010, *Phys. Rev. A*, 82, 042715
- Larsson, M. 2000, in *Phil. Trans. R. Soc. Lond. A*, Vol. 358, *Astronomy, physics and chemistry of H⁺₃*, 2433–2444
- Laubé, S., LePadellec, A., Sidko, O., et al. 1998, *Journal of Physics B Atomic Molecular Physics*, 31, 2111
- Le Bourlot, J., Pineau des Forets, G., & Roueff, E. 1995, *A&A*, 297, 251
- Lee, H.-H., Herbst, E., Pineau des Forets, G., Roueff, E., & Le Bourlot, J. 1996, *A&A*, 311, 690
- Lee, H.-H., Roueff, E., Pineau des Forets, G., et al. 1998, *A&A*, 334, 1047
- Lindsay, C. M. & McCall, B. J. 2001, *Journal of Molecular Spectroscopy*, 210, 60

- Liszt, H. S. 2006, Royal Society of London Philosophical Transactions Series A, 364, 3049
- McCall, B. J., Geballe, T. R., Hinkle, K. H., & Oka, T. 1998, *Science*, 279, 1910
- McCall, B. J., Hinkle, K. H., Geballe, T. R., et al. 2002, *ApJ*, 567, 391
- McCall, B. J., Huneycutt, A. J., Saykally, R. J., et al. 2004, *Phys. Rev. A*, 70, 052716
- McCall, B. J., Huneycutt, A. J., Saykally, R. J., et al. 2003, *Nature*, 422, 500
- McElroy, D., Walsh, C., Markwick, A. J., et al. 2013, *A&A*, 550, A36
- McKee, C. F. & Ostriker, E. C. 2007, *ARA&A*, 45, 565
- Öberg, K. I., Linnartz, H., Visser, R., & van Dishoeck, E. F. 2009a, *ApJ*, 693, 1209
- Öberg, K. I., van Dishoeck, E. F., & Linnartz, H. 2009b, *A&A*, 496, 281
- Oka, T. 2004, *Journal of Molecular Spectroscopy*, 228, 635
- Oka, T. 2013, *Chemical Reviews*, 113, 8738
- Okumura, M., McCall, B. J., & Geballe, T. R. 2013, *The Journal of Physical Chemistry A*, 117, 9305
- Pagani, L., Roueff, E., & Lesaffre, P. 2011, *ApJ*, 739, L35
- Pagani, L., Vastel, C., Hugo, E., et al. 2009, *A&A*, 494, 623
- Pan, L. & Padoan, P. 2009, *ApJ*, 692, 594
- Petrignani, A., Altevogt, S., Berg, M. H., et al. 2011, *Phys. Rev. A*, 83, 032711
- Plašil, R., Glosík, J., Poterya, V., et al. 2002, *International Journal of Mass Spectrometry*, 218, 105
- Price, R. J., Viti, S., & Williams, D. A. 2003, *MNRAS*, 343, 1257
- Quack, M. 1977, *Molecular Physics*, 34, 477
- Rachford, B. L., Snow, T. P., Destree, J. D., et al. 2009, *ApJS*, 180, 125
- Rachford, B. L., Snow, T. P., Tumlinson, J., et al. 2002, *ApJ*, 577, 221
- Rimmer, P. B., Herbst, E., Morata, O., & Roueff, E. 2012, *A&A*, 537, A7
- Savage, B. D., Bohlin, R. C., Drake, J. F., & Budich, W. 1977, *ApJ*, 216, 291
- Semenov, D., Hersant, F., Wakelam, V., et al. 2010, *A&A*, 522, A42
- Semenov, D., Wiebe, D., & Henning, T. 2006, *ApJ*, 647, L57
- Sipilä, O., Caselli, P., & Harju, J. 2013, *A&A*, 554, A92

- Snow, T. P. & McCall, B. J. 2006, *ARA&A*, 44, 367
- Spaans, M. 1996, *A&A*, 307, 271
- Sternberg, A. & Neufeld, D. A. 1999, *ApJ*, 516, 371
- Talbi, D. & Saxon, R. P. 1988, *J. Chem. Phys.*, 89, 2235
- Tom, B. A., Zhaunerchyk, V., Wiczer, M. B., et al. 2009, *J. Chem. Phys.*, 130, 031101
- van der Tak, F. F. S. 2006, *Royal Society of London Philosophical Transactions Series A*, 364, 3101
- van der Tak, F. F. S. & van Dishoeck, E. F. 2000, *A&A*, 358, L79
- van Dishoeck, E. F. 1987, in *IAU Symposium, Vol. 120, Astrochemistry*, ed. M. S. Vardya & S. P. Tarafdar, 51–63
- van Dishoeck, E. F., Jonkheid, B., & van Hemert, M. C. 2006, *Faraday Discussions*, 133, 231
- Varju, J., Hejduk, M., Dohnal, P., et al. 2011, *Physical Review Letters*, 106, 203201
- Walmsley, C. M., Flower, D. R., & Pineau des Forêts, G. 2004, *A&A*, 418, 1035
- Watanabe, N., Kimura, Y., Kouchi, A., et al. 2010, *ApJ*, 714, L233
- Webber, W. R. 1998, *ApJ*, 506, 329